Effective extrusion-based 3D printing system design for cementitious-based materials

5 authors, including:

Abdulrahman Albar
Brunel University London
9 PUBLICATIONS 347 CITATIONS

SEE PROFILE

Mehdi Chougan
Brunel University London
45 PUBLICATIONS 1,005 CITATIONS

SEE PROFILE

Mazen Al-Kheetan
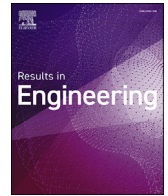Mu'tah University
60 PUBLICATIONS 1,036 CITATIONS

SEE PROFILE

M. Rafiq Swash
Brunel University London
69 PUBLICATIONS 705 CITATIONS

SEE PROFILE

Effective extrusion-based 3D printing system design for cementitious-based materials

Abdulrahman Albar [a], Mehdi Chougan [b], Mazen J. Al- Kheetan [c], Mohammad Rafiq Swash [a], Seyed Hamidreza Ghaffar [b,*]

[a] Department of Electronic and Electrical Engineering Brunel University London Uxbridge, United Kingdom
[b] Department of Civil and Environmental Engineering Brunel University London Uxbridge, United Kingdom
[c] Civil and Environmental Engineering Department, College of Engineering, Mutah University, P.O. Box 7, Mutah, Karak, Jordan

ARTICLE INFO

ABSTRACT

The widespread popularity of additive manufacturing in most industries ranging from biomedical to aerospace suggests a transformation in manufacturing, which has recently also emerged in the construction sector. This paper presents an active system for the extrusion-based 3D printing of cementitious materials. The system can be extended to other materials and scaled up with slight hardware modifications. The proposed system uses an unconventional yet simplistic approach to generate a consistent output of material throughout the printing process. The effectiveness of the extruder is demonstrated through an extensive printing and testing of various cementitious-based materials. The printing and material parameters, which are essential for high mechanical strength printed object were investigated and optimized through a logical iterative loop of trials. The results showed the shape retention of 3D printed objects using the proposed design of extrusion-based system in conjunction with optimized rheology of cementitious-based materials was encouraging for larger scale 3D printing.

Introduction

Additive manufacturing is becoming one of the fastest developing key instruments in the construction industry. The term Additive manufacturing (AM), popularly known as 3D printing, is the process of additively joining materials to make a physical 3D object from a digital 3D model [1]. Several AM technology methods, including fused deposition modeling (FDM), selective laser melting (SLM), Stereolithography (SLA), and digital light processing (DLP) have been adopted [2]. A variety of metals, polymers, composites, and ceramics can be utilized for AM, although, the use of these feedstock is dependent on the type of AM process used [3–5].

Some of the benefits of deploying AM in the construction sector are its ability to print complex geometric shapes with minimum waste, which makes it a cost-effective solution for the construction industry [6]. The construction industry so far has been developed around two leading AM technologies, the extrusion-based AM method, with some effort on developing a scaled-up 3D printing technology for cementitious materials. Existing additive manufacturing systems were originally devolved

for small-scale products prototyping. The greatest challenge that the construction sector faces is the scaling up of existing AM technologies. The gantry solution simply represents a direct scaling-up of AM to additive construction – in other words a giant 3D printer [7,8]. In a gantry system, a set of motors are controlled in any direction defined by along the X, Y and Z-axes in Cartesian coordinates. Gantry solutions were first developed for concrete extrusion in 2001, and Khoshnevis et al. from the University of South California in the US patented the combination of this solution with the material process under the name "Contour Crafting" [9]. Contrasting Contour Crafting, where the focus had always been on entire constructions fabricated in one-piece, Freeform Construction focuses on the fabrication of full-scale construction components such as walls and panels [10]. This system works on the same principle as Contour Crafting and includes a printing head digitally controlled by a CNC machine to move in the X, Y and Z directions along three chain-driven tubular steel beams. A material hopper was mounted on top of the printing head and was connected to a pump that carried the material to the printing nozzle [11].

There are two principal components of any extrusion-based 3D

printer, (i) the extruder assembly and (ii) the positioning system. The extruder's ability to accurately deposit the precise quantity of material over varying distances is fundamental to the printing process and final output. However, accuracy of the extruded material is not significant when the positioning system is not accurate. Therefore, both the positioning system and the extruder are needed to build a visually and geometrically accurate structure. The positioning and delivery system are usually standard machinery, i.e. gantry or robotic arm and a mortar pump for delivering the materials to the nozzle. The extruder and delivery systems have the most significant influence on whether or not extrusion printing will produce a successfully printed object [12]. Hence, this paper proposes a robust active extrusion nozzle system design and a printing platform that enables the 3D printing of various cementitious materials. The 3D printing system designation contains an Extrusion system design including Nozzle design, Hopper prototype, scraper design, and positioning system design. The proficiency of the presented system was assessed by printing three geopolymers mixtures with low (i.e. Mix-1), medium (i.e. Mix-2), and high (i.e. Mix-3) printability ranges in terms of flow-ability, setting time, and open time. The effects of adopted printing system was investigated by inspecting each printed sample's shape retention and comparison between the properties of printed specimens and conventionally casted counterparts in terms of density, flexural and compressive strength. Moreover, the buildability test of the selected mix was conducted in 25 subsequent layers to assess the capacity of the designed system to print medium-scale structures.

Extrusion system design

The extrusion system of 3D printer is an extremely important part of the overall AM process. Many parameters influence the extrusion of cementitious-based materials.

In this study, the design of the hopper and extrusion system was a result of an iterative trial and error method based on cementitious-based material rheology, e.g. workability, flow-ability and extrudability.

Fig. 1 a shows the sketch for the extrusion system. The design includes a hopper to feed in the material, an extrusion auger screw to transport materials down and through the nozzle, the nozzle that shapes the material extrusion output and a geared motor to drive the screw. Additionally, a scraper is added to agitate the material and aid with extrusion reliability. Fig. 1b and c shows the CAD drawing of the proposed extrusion hopper. The barrel's diameter of 37 mm is chosen based on the auger screw used for this study. However, the hopper slopes angles were explicitly designed to try to achieve a mass flow pattern, as illustrated in Fig. 1d and e. For many materials, flow problems such as erratic flow, materials segregation, and particle degradation in stagnant regions can be eliminated by ensuring that a mass flow pattern exists in the hopper [13]. Given the nature of the printed cementitious material and the

importance of keeping its homogeneity, the hopper design avoids any sharp or steep edges that add unnecessary pressure to the mixture ensuring a smooth flow to and out of the nozzle. Fig. 1b illustrates a transparent rendered view of the proposed extrusion system. While Fig. 1c shows an assembled rendered view of the extrusion system attached to the Open build rail, which will then be attached to the positioning platform.

Hopper prototype

The implementation of the design was possible by using sheet metal fabrication. The hopper was designed using Autodesk Inventor, and then laser cut using a plasma machine, as shown in Fig. 2a. The 1.5 mm thick stainless-steel sheet is then bent to shape and welded together, as shown in Fig. 2b.

Scraper

A form of agitation tool is required to obtain a suitable extrusion for the concrete like materials, e.g. non-Newtonian, pseudo-plastic fluid with a typical shear thinning behavior [14]. Agitation contributes to the pump-ability of the cementitious materials by lowering the effective shear stress due to the reduction in the friction of the internal particles [15]. Hence, a scraper was designed and implemented to the hopper, as shown in Fig. 3. The scraper creates a further mixing effect of the materials inside the hopper and scrapes the sides to completely discharge
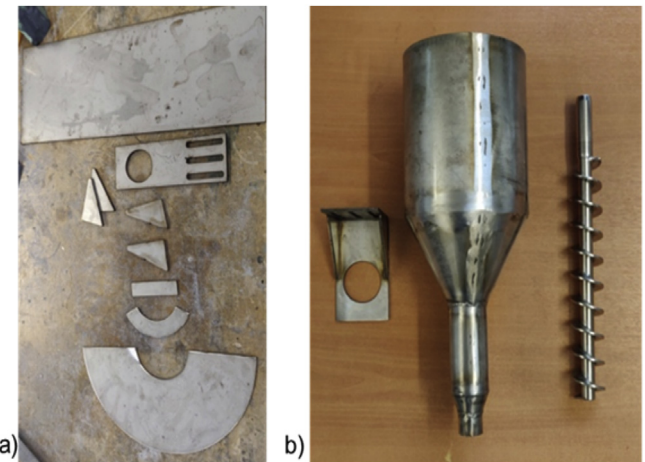

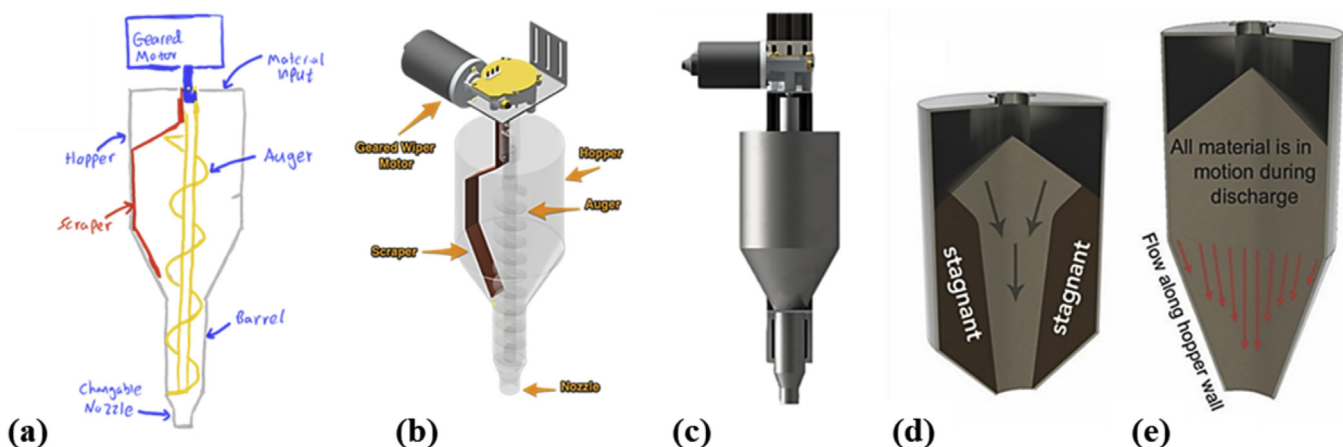**Fig. 2.** (a) Plasma cut sheet metals for the proposed hopper and (b) proposed hopper prototype.

Fig. 1. (a) Proposed extrusion system idea sketch, (b) transparent render of the proposed extrusion and (c) assembled render; (d) funnel flow; (e) mass flow.
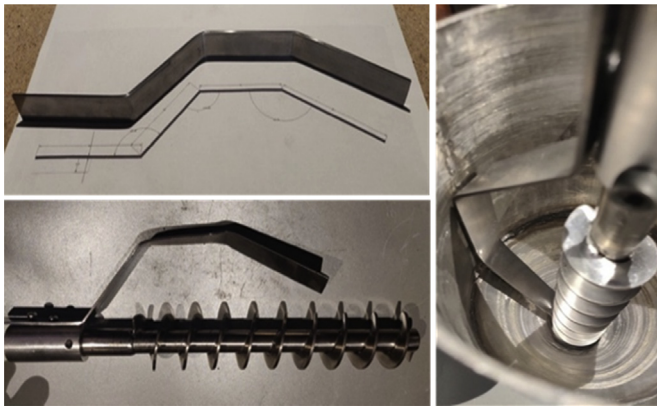
Fig. 3. The implementation of the scraper design into the hopper.

the cementitious materials. Therefore, it can be used as a stand-alone extrusion system without an external pump for small to medium-sized prints. The scraper is an integral part of the extrusion system with the potential of adding a vibration motor to further improve the flow-ability and compactness of the cementitious-based materials. Additionally, it prevents clogging of nozzle.

Nozzle design

In order to achieve a successful print, the nozzle size plays a remarkable role in shaping the materials output and determining the buildability of the final structure. Based on the designed object, e.g. its dimension and necessary resolution, the nozzle size can be modified to a smaller or a larger size. Fig. 4a shows the circular nozzle including a holder, upper and lower nozzle and barrel clamp. This system gets attached to the hopper's barrel which can simply be attached and detached. Fig. 4b illustrates different upper nozzle sizes used in this study to examine the best performing nozzle size for the cementitious based materials printing.

To select the optimum nozzle size, two samples were printed for each nozzle dimeter as seen in Fig. 5. **The first one is a rectangular shaped sample (Fig. 5 a,b,c)** that is used to assess the ability of the nozzles to stack layers on top of each other without collapsing (i.e. the buildability of the nozzle). The second sample (Fig. 5 d,e,f) is determining the extrusion width produced by each nozzle and the details they are capable of printing. The printed objects were printed continuously in a zigzag road map. The smaller dimeter of the nozzle leads to finer details of printed objects. However, this comes at the cost of a lower buildability factor as observed in Fig. 5a. On the other hand, a larger nozzle will

produce a courser structure but an improved buildability. Throughout this study, the 20 mm nozzle was used to achieve the best buildability results.

Positioning system design

The second fundamental system that is needed to produce geometrically and vitally accurate printed objects is the positioning system. The positioning system used in this study, is a modified CNC gantry system, based on the open source extrusion rails Open-Builds platform (Workbee CNC by OOZNEST - UK). The platform is designed to print small to medium concrete samples for the purpose of developing a sustainable concrete mixture for 3D printing. Thus, a reasonable print area is required to print samples and small structure. Hence, the printer working area is; 490 x 400 x 300 mm, which is a sufficient to examine mechanical properties and buildability of printed samples. The gantry is a Cartesian XYZ platform, with the axes driven by NEMA 23 Stepper motors, UK coupled with TB6600 drivers. The drivers are controlled using a RAMP board which is a common 3D printers controller based on an Arduino Mega 2560 microcontroller, UK that communicates to a PC over a serial port. The open source firmware used to control the board is Klipper. Fig. 6 shows the final implantation of the positioning system with the control unit.

Printing path and parameters

Printing path, gantry speed, extrusion rate, and layer height are known as basic 3D printing process parameters. In this study, in order to come up with the optimal printing parameters, various 3D models were designed. Initially, a 150x150x100 mm rectangular path (Fig. 7a) was 3D printed in order to investigate the other printing parameters such as; gantry motion speed, layer height or printing resolution and extrusion rate. It should be noticed that for all the experiments the nozzle size was set to 20 mm, as it produced the best flow rate with the geopolyemers. The objects 3D prints were conducted with a printer head speed of 30 mm/s, layer height of 15 mm, and an extrusion rate of 50% (see Fig. 7a). As it can be observed, the primary settings led to unsuccessful print, which was because of the large layer height. Therefore, the settings were adjusted, i.e. decreasing the speed to 20 mm/s, and the layer height to 10 mm but keeping the same extrusion rate, led to successful print, shown in Fig. 7b. It is worth mentioning that the extrusion rate, controlled by speed of extruder's motor, will vary depending on the consistency of mixture throughout testing. Fig. 7c, presents a smaller rectangular block measuring 180x80x60 mm, that shows good buildability and shape stability. Nevertheless, a cyclic effect is evident on the middle-printed layers. This phenomenon is also observed quite commonly in polymer 3D printing extrusion systems and is typically triggered by a partially
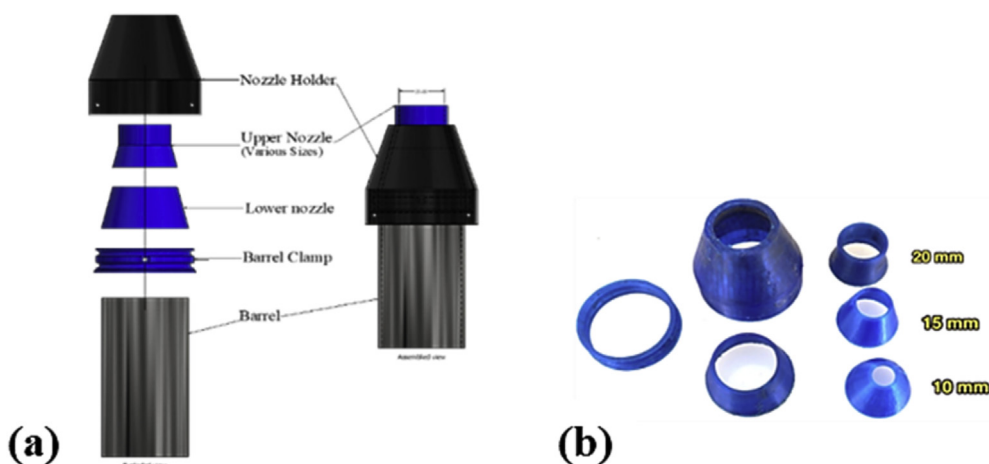

Fig. 4. (a) detailed assembly drawing of the proposed nozzle, (b) prototyped nozzles using 3D printing.
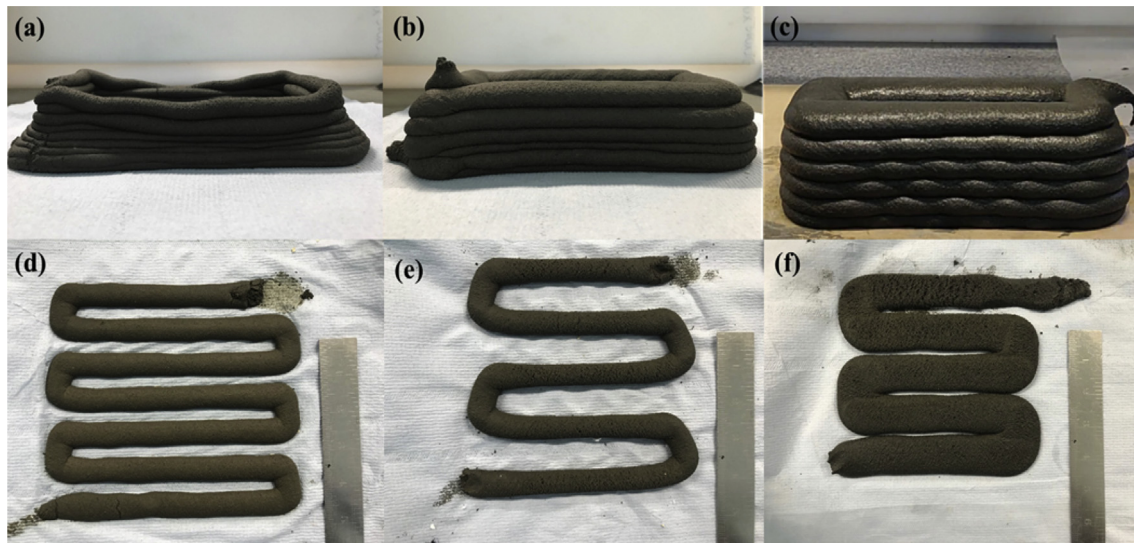
Fig. 5. Printed samples using various nozzles dimeters (a,d) using a 10mm nozzle (b,e) 15 mm nozzle and (c,f) 20 mm nozzle.
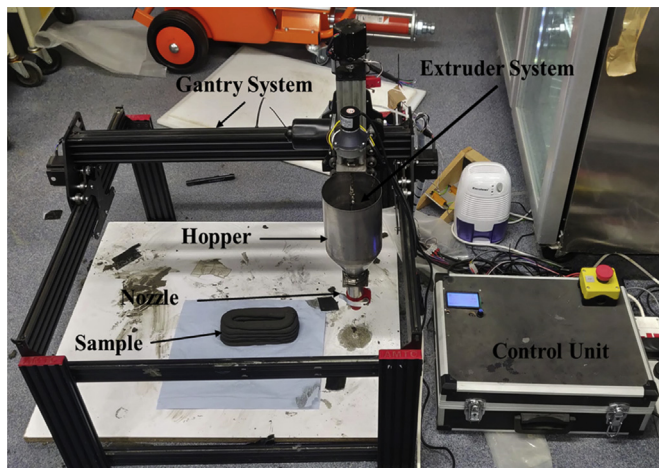

Fig. 6. Positioning system with the control unit.

filled section on the screw [16]. In order to reduce the rhythmic surges, improved synchronisation of gantry speed, extrusion rate are required, and alternatively redesigning of the screw could be beneficial in eliminating this phenomenon.

Cementitious-based materials for printing

Several additives incorporation have been proposed to improve the mechanical and physical performance of Ordinary Portland cement-based composites [17,18], however, the never-ending production of cement has amplified the amount of CO_2 being released, which contributes to the issue of global warming and climate change [19]. Therefore, a more sustainable approach using the existing admixtures to replace conventional Ordinary Portland cement-based composites is of vital importance. Various researchers have carried out many studies on geopolymer composites [20–22], which exhibit similar or better structural load bearing capacity and durability when compared to conventional concrete. Ordinary Portland cement is generally not required in the manufacturing process of geopolymer concrete. The main ingredients of geopolymer are: (i) alkaline solutions including sodium hydroxide (NaOH), sodium silicate (Na_2SiO_3), potassium hydroxide (KOH), or potassium silicate (K_2SiO_3), (ii) aluminosilicate sources of by-product materials including ground granulated blast furnace slag (GGBS) and fly ash (FA), and (iii) fine and coarse aggregates.

For this study, the as-received materials, including (i) Fly ash (FA) (Cemex, UK) following the BS EN 450-1:2012; (ii) Ground-granulated blast furnace slag (GGBS) (Hanson UK); (iii) Silica fume (SF) (J. Stoddard & Sons Ltd); (iv) Sodium silicate (Na_2SiO_3) (Solvay SA, Portugal); and (v) sodium hydroxide 98% NaOH (Fisher Scientific, Germany), were used for preparing the geopolymers. The microstructure morphology and physical state of each as received materials, including FA, GGBS, and SF, were assessed by employing a scanning electron microscope (SEM) (Supra 35VP) and reported in Fig. 8a-c.

Mixing procedure and design formulations

In order to assess the compatibility evaluation of the designed system in terms of extrusion and printing the geopolymers, three geopolymer mixes (see Table 1) were prepared. The total activator content (NaOH + Na_2SiO_3) was 18% by the weight of the binder for all the mixtures. In this study, the GGBS and SF content ranged between 15-35% and 5-15%, respectively, by the total weight of binder (FA+GGBS+SF). For Mix 3, the SF and GGBS dosage reduction was substituted by increasing the FA dosage by 70%. The oven-dried river sand was firstly sieved and then added to the binder (sand/binder ratio: 0.55) with the size range of 40% of grade 0-0.5mm and 60% of 0.5-1mm for Mix 1, 3, and substituted to 40% of grade 0.5-1mm and 60% of grade 0-0.5mm for Mix-2. The materials were dry mixed for 2 min using a domestic mixer device (Kenwood, Germany) at 250 rpm. The sodium hydroxide and sodium silicate solutions were mixed up for 5 min at 700 rpm with the constant ratio of Na2SiO3: NaOH = 2:1 in order to achieve the alkali-activator. Finally, the activator liquid solution was gradually incorporated to the dry materials, and the resulting paste was stirred at different mixing rates to form a homogeneous geopolymer mixture. Six samples of 40 x 40 x 160 were prepared for each mixture, including, three samples for the conventionally casted specimens and three samples for the printed parts utilizing the designed 3D printer extruder. All the samples were first preserved in a controlled environment at 60 °C for 24 h immediately after the demolding and printing process, followed by keeping them at ambient temperature (i.e. 20 °C) for seven days.

Testing of cementitious-based materials

Fresh properties

Several tests have been conducted to evaluate the flow-ability of geopolymers before commencing the printing process. Flow table test was assessed following the BS EN 1015-3:1999 and IS 4031(Part 7):1988
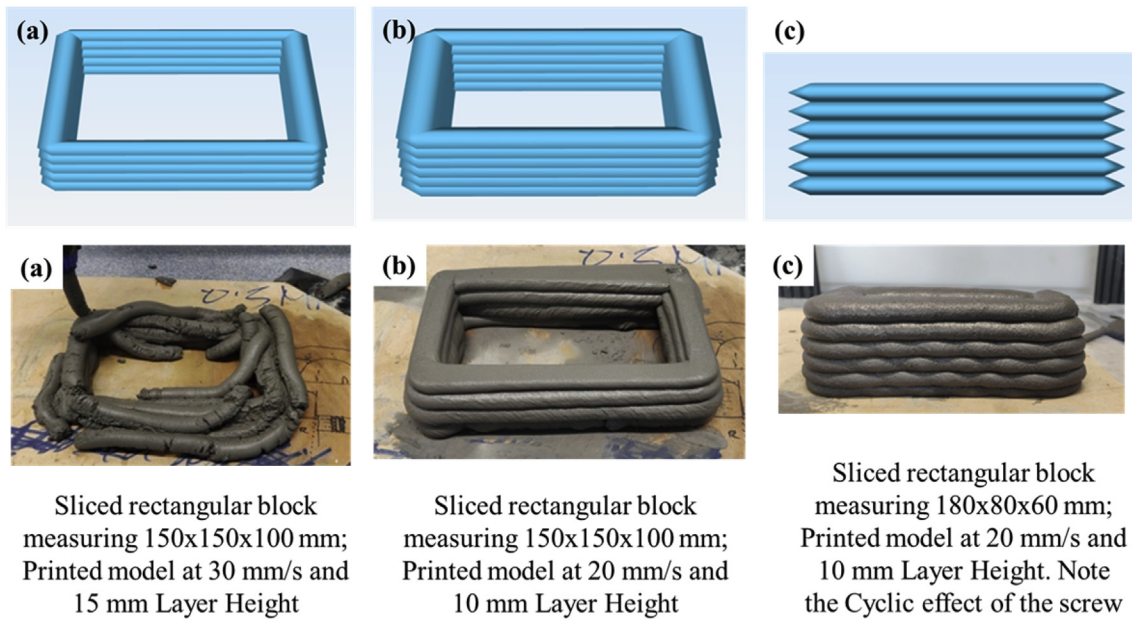
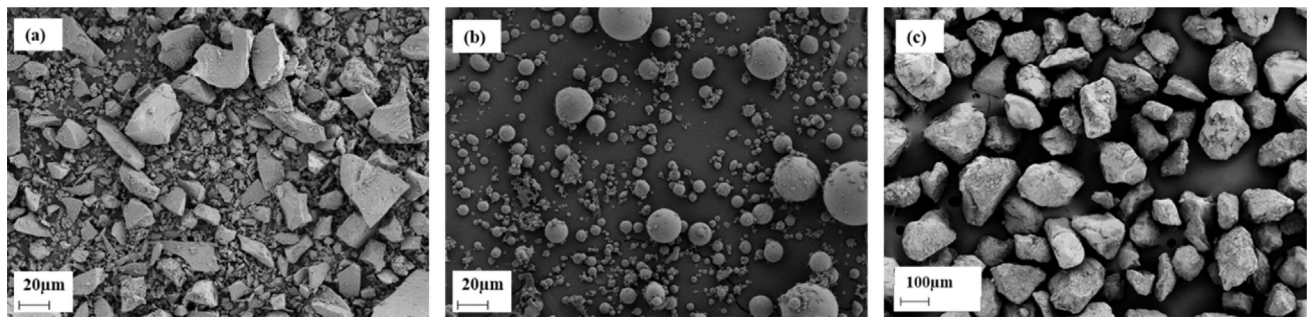Fig. 7. Initial printed parts using the proposed systems.

Fig. 8. Microstructure of as-received aggregates, (a) GGBS, (b) FA, and (c) micro-SF.

Table 1
Mix design formulations.

Mixture Name	Binder			Aggregate		Na$_2$SiO$_3$: NaOH ratio
	FA Wt %	GGBS Wt%	SF Wt %	0-0.5mm Wt%	0.5-1mm Wt%	
Mix-1	60	35	5	40	60	2:1
Mix-2	60	25	15	60	40	2:1
Mix-3	70	15	15	40	60	2:1

to evaluate the flow-ability of fresh mixtures. In this test, the mould apparatus placed at the centre of the flow table disc was filled with two subsequent layers of geopolymer. After 20 s, the mould apparatus was removed gently in a vertical direction, and the flow table was jolted continuously every one minute for 15 times. The results were recorded by measuring the spread of geopolymer in two perpendicular directions employing calliper after 0, 5, and 15 min, using the following equation.

$$Flow \quad (\%) = \frac{D_{avg} - D_0}{D_0} \times 100 \tag{1}$$

The Vicat test was defined the setting time of the fresh mixtures following the BS EN480-2:2006. For each composition, the Vicat apparatus was filled with geopolymers paste. The penetration of a Vicat needle (1mm diameter) in the fresh geopolymer was visually measured every 3 min until the needle penetration reached 4 mm.

The open time test was performed by the simple-line printing of geopolymers in a dimension of 250mm x 24mm in a periodic resting time of 5 min until the discontinuity of the printed line occurred. This test method completely shows the period that the fresh geopolymers show acceptable workability for the printing process.

Shape retention was evaluated to understand the capability of the designed extruder to print the wide range of geopolymer in terms of flow-ability, open time, and setting time. In this regard, six subsequent layers of geopolymer paste were printed, and then the printed sample was allowed to set for approximately 60 min. After setting the printed object, the appearance of each sample was visually examined.

The rheology tests were carried out to evaluate the fluidity of fresh geopolymers using KinexusLab + rheometer (Malvern Instruments Ltd., UK) equipped with the rSpace software (Malvern Panalytical Ltd, UK) immediately after mixing. The rheological terms, including shear stress (t) and apparent viscosity (η) versus shear rate (γ) (varied between 0.1 s-1 and 30 s-1 over 22 intervals), were recorded. Due to the non-Newtonian nature and pseudoplastic behaviour of fresh geopolymer mixtures [23], modified-Bingham model (MBM) was selected among several other fitting models [14,24,25] (i.e. Bingham model (BM) and Herschel–Bulkley model (HB)) to accurately calculate the rheology parameters of geopolymers (i.e. Yield shear stress (τ0) and plastic viscosity (ηp)).

$$\tau = \tau_0 + \eta_p \cdot \gamma + c\gamma^2 \tag{2}$$

Mechanical properties

According to BS EN 196-1:2016, the mechanical property (i.e. flexural and compressive strength) of each mixture (three specimens for each mix), both casted and printed, were evaluated after seven days of curing. Universal testing machine (Instron 5960, United Kingdom) equipped with 150kN load cell at a constant loading rate of 1 mm/min, with the perpendicular loading direction to the printing path. Moreover, the density of each mixture was calculated by weight and volume measurements by using a digital caliper and an analytical balance (Mettler-Toledo Ltd.).

Research plan

Fig. 9 illustrates the strategy for this study. The work started in parallel for extruder and geopolymer mix design. The steps required for each of the designs were critically evaluated through various individual tests in order to move to the printing trials and error stage.

Results and discussions

Fresh properties

The fresh properties of geopolymers including, shape stability, workability, and flow-ability are the most critical factors for successful 3D printing, which can be modified by changing the features of aggregates (i.e. shape, size, surface textures and gradation, and the volume fraction) [26]. It can be seen that all the fresh properties of geopolymers, including flow table, setting time, and open time are linked together. In this study, the minimum and the maximum flow-ability values was registered by Mix-1 and Mix-3 (see Fig. 10a), with an initial (i.e. 0 min) flow-ability of 23% and 52%, respectively. The results also indicated that by replacing GGBS with FA and SF, the mixtures' setting time was considerably increased from 12 to 47 min for Mix-1 to Mix-3, respectively. The open time test results (Fig. 10c) shows a gradual increase from 10 to 35 min for Mix-1 to Mix-3, respectively. Moreover, the setting time results also show a similar trend, increasing from 10 to 40 min for Mix-1 to Mix-3, respectively (see Fig. 10b).

Fig. 10d shows the plastic viscosity and yield shear stress of geopolymers. The results revealed that the selected geopolymers have different rheological parameters that are correlated to their fresh properties. Mix-1 showed a maximum yield shear stress and plastic viscosity values (i.e. 56.29 Pa and 17.06 Pa·s), and they gradually decreased to 41.56 Pa and 16.46 Pa·s for Mix-2, and 25.98 Pa and 8.75 Pa·s for Mix-3, respectively.

The fresh property enhancement of geopolymers can be generated by the decrease in the content of GGBS in geopolymers, which prevents the rapid setting of the mixtures. Lampropoulos et al. and Xie et al. also indicated that the high dosage of GGBS increases the CaO content in the mixtures, which leads to forming the gel components (i.e. C–S–H and the 3D stable silico-aluminate structure) by the early-age geopolymerization [27,28]. On the other hand, the substitution of angular shape GGBS particles with rounded and spherical shape particles (i.e. FA and SF), works on reducing the cohesiveness of paste and induces a lubrication effect within the mixture [26,28,29].

In order to assess the efficiency of the designed system, all the geopolymers with different fresh properties have been tested by visually monitoring the shape retention of the printed parts, which is essential to evaluate the printing performance of the designed system. The results revealed that the extrusion system is able to print a variety of mixtures with both high and low flow-ability without any restrictions. however, the shape retention of printed layers were not adequate for upscaling and printing larger objects. As can be seen in Fig. 11, The best performance in shape retention was recorded for Mix-2 concerning the other geopolymers (i.e. Mix-1 and Mix-3) both for the first layer height (i.e. 7.5mm) and the difference between the first layer and last layer height (i.e. 14.5 – 7.5 = 7 mm). This could be attributed to the optimum values of Mix-2 in setting time and open time (i.e. 33 and 20 min, respectively) which contributes to stabilizing its shape during the deposition of the upper subsequent layers.

Mechanical properties of cementitious-based materials

Mechanical performance (i.e. compressive and flexural strength) and the density of each geopolymer mix in both conventionally casted and printed samples have been measured and compared (see Fig. 12a-c).

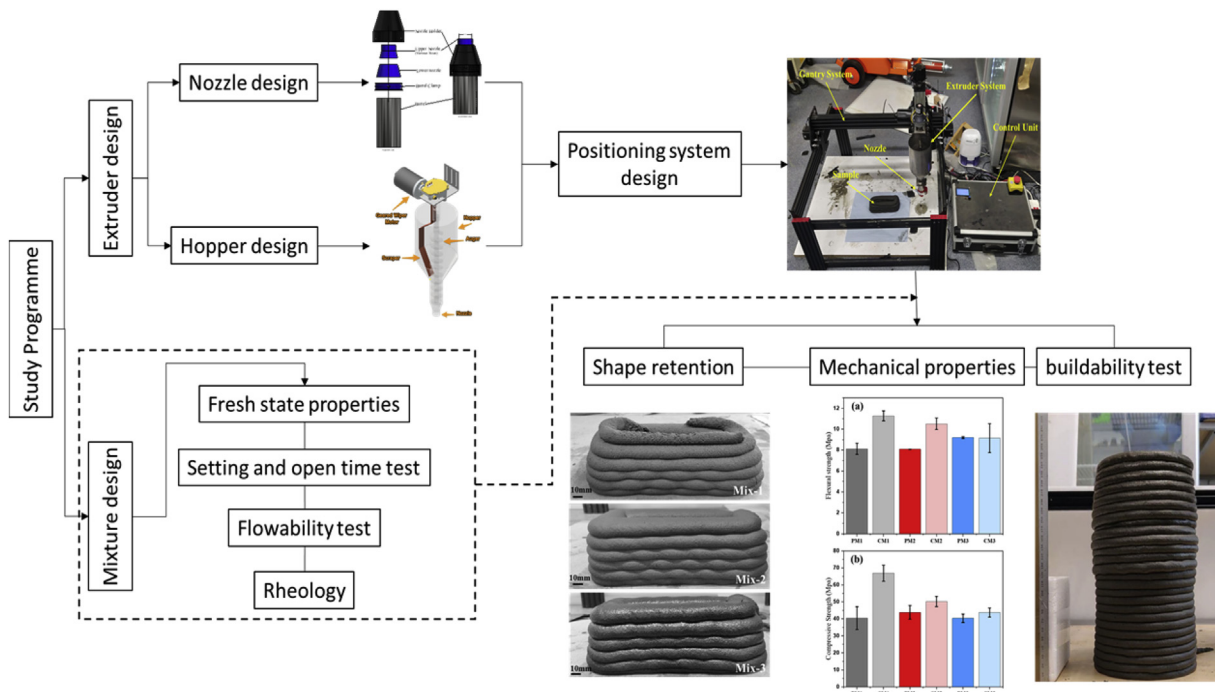The flexural and compressive strength evaluation of 3D printed and

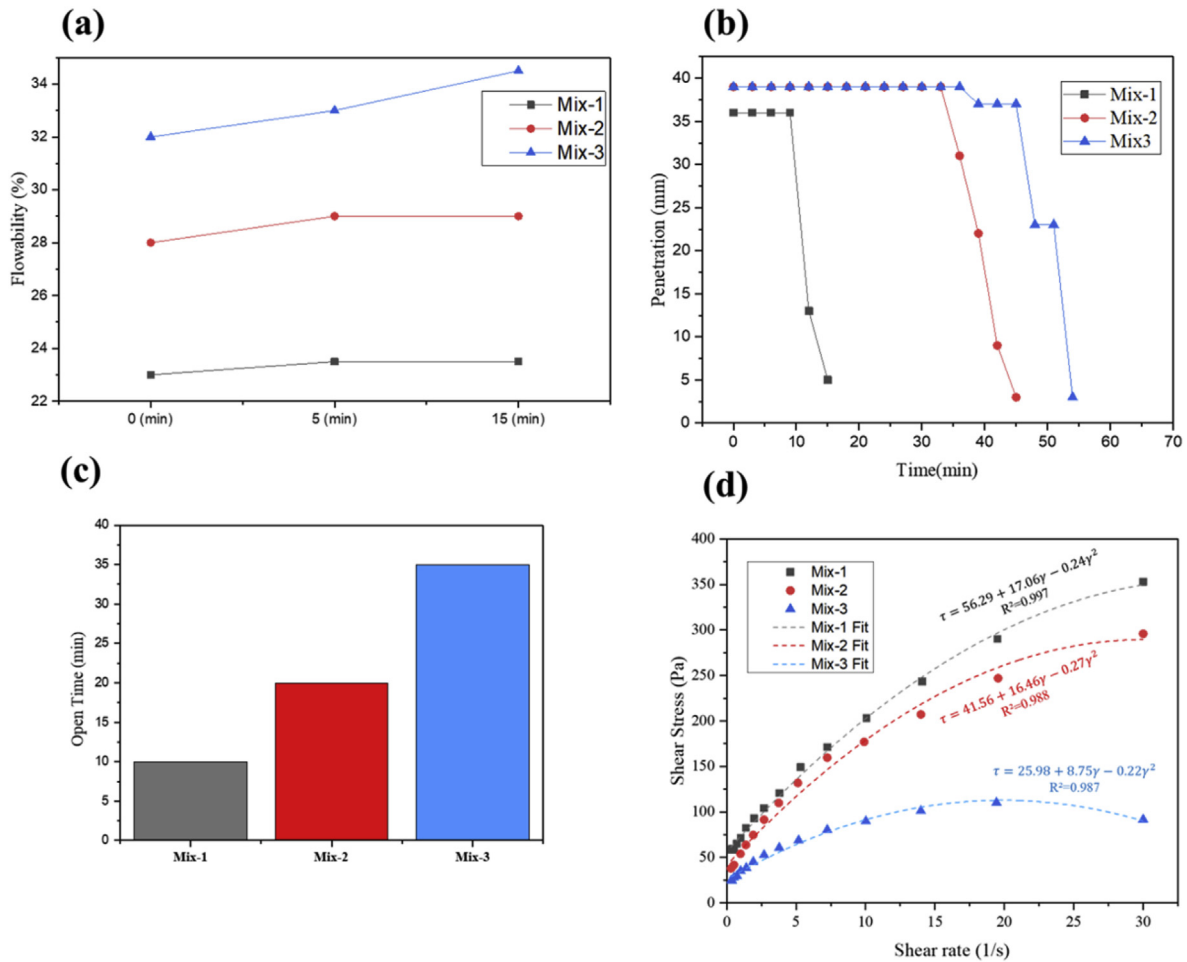**Fig. 9.** Experimental framework and testing programme.

Fig. 10. Fresh properties of designed geopolymers; (a) Flow-ability, (b) setting time, (c) open time, and (d) rheology test.

Fig. 11. Shape-retention ability of geopolymer composites.

casted specimens (Fig. 12a, c) in the perpendicular direction of load indicated that the flexural strength of the 3D printed samples is lower or comparable to that of casted samples. The density evaluations also revealed that the density gap between the casted and printed sample has changed by decreasing the GGBS content in which for Mix-1, the density values of the casted sample is higher than printed samples (i.e. 2.12 g/cm³ for CM1 and 2.06 g/cm³ for PM1). In contrast, for the other mixtures, the density of printed samples is higher than that of casted samples. The outcomes are completely aligned with the results reported by Panda et al., which indicated that the high-pressure application during the extrusion process increases the density from 1500 kg/m³ for casted specimens to 2050 kg/m³ for geopolymer 3D printed samples [30]. The results are evident that by decreasing the GGBS content, the mechanical property gap between the casted and printed samples decreased. This could be assessed by the gradual increase in setting time and flow-ability of geopolymers from Mix-1 to Mix-3 (see Fig. 10 a-b), which facilitate the compaction during the extrusion process, leads to the higher porosity

refinement and densification concerning the conventionally casted samples [31]. Moreover, the flexural and compressive strength of conventionally casted samples decreased from 11.3 and 66.9 MPa for Mix-1(i.e. CM1) to 10.5 and 50.3 MPa for Mix-2 (i.e. CM2) and 9.1 and 43.7 MPa for Mix-3 (i.e. CM3), respectively. According to Xie et al., the reason could be due to the decrease in sodium aluminosilicate (N-A-S-H) and calcium aluminosilicate (C-A-S-H) dosage in the mixture as a result of GGBs dosage reduction which prevents the formation of dense structure [27].

Finally, after identifying the appropriate feedstock (i.e. Mix-2) in terms of adequate flow-ability, mechanical property, shape stability, and buildability, the designed 3D printer and extrusion system were utilized to perform the buildability test. The outcomes revealed that the developed system is able to correctly print the object in 25 subsequent layers with approximately 250 mm height (see Fig. 13). The better shape stability of the first layer (i.e. 8.7mm) can act as a base to tolerate the upper layer's weight and, consequently, resulting in better presentation of this
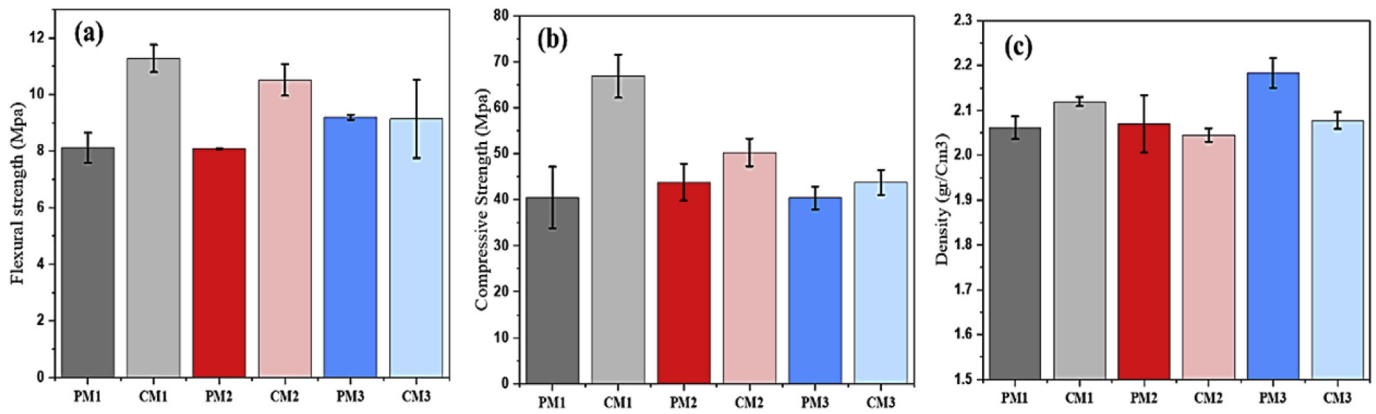
Fig. 12. Mechanical performance and density of PM (printed) and CM (casted) geopolymers, (a) flexural strength, (b) compressive strength, and (c) density.

Fig. 13. Buildability test of Mix-2 with the designed 3D printer system.

mixture for printing the large-scale structures [22].

Conclusions

The main objective of this paper was to develop an extrusion-based 3D printing system that enables geopolymeric cementitious-based materials in a variety of printability ranges to be tested without using expensive equipment such as robotic arms.

The results of this paper elucidate the capability of the designed extruder and positioning system to print the full range of cementitious materials with high (i.e. Mix-3), medium (i.e. Mix-2) and low (i.e. Mix-1) flow-ability. Moreover, the proposed designed extruder is able to compress the fresh cementitious mixture during the extrusion process, densify the printed object, which subsequently leads to a decrease in the flexural and compressive strength gap between printed and conventionally casted samples in the hardened state.

An adequate medium-scale object (i.e. 25 layers, 250mm height) without any disruption and collapse was printed using the designed 3D printing system. The optimized printing parameters, were: nozzle size of 20mm, gantry speed of 20 mm/s, layer height of 15 mm, and an extrusion rate of 50%, On the other hand, the optimum mix i.e., Mix-2, illustrated the optimum fresh and hardened properties (i.e. 20 min for open time, 33 min for setting time, 8.1 MPa for flexural and 43.8 MPa for compressive strength).

CRediT authorship contribution statement

Abdulrahman Albar: Formal analysis, Writing - original draft, Data curation. **Mehdi Chougan:** Formal analysis, Writing - original draft, Data curation. **Mazen J. Al- Kheetan:** Writing - review & editing. **Mohammad Rafiq Swash:** Writing - review & editing. **Seyed Hamidreza Ghaffar:** Conceptualization, Methodology, Supervision, Writing - review

& editing.

References

[1] D. Delgado, P. Clayton, W.J.O. Brien, C. Seepersad, M. Juenger, R. Ferron, S. Salamone, Applications of additive manufacturing in the construction industry – a forward-looking review, Autom. ConStruct. 89 (2018) 110–119, https://doi.org/10.1016/j.autcon.2017.12.031.

[2] V. Petrovic, J. Vicente Haro Gonzalez, O. Jordá Ferrando, J. Delgado Gordillo, J. Ramón Blasco Puchades, L. Portolés Griñan, Additive layered manufacturing: sectors of industrial application shown through case studies, Int. J. Prod. Res. 49 (2011) 1061–1079, https://doi.org/10.1080/00207540903479786.

[3] S. Ford, M. Despeisse, Additive manufacturing and sustainability: an exploratory study of the advantages and challenges, J. Clean. Prod. 137 (2016) 1573–1587, https://doi.org/10.1016/j.jclepro.2016.04.150.

[4] S. Hamidreza, J. Corker, M. Fan, Automation in Construction Additive Manufacturing Technology and its Implementation in Construction as an Eco-Innovative Solution, vol. 93, 2018, pp. 1–11, https://doi.org/10.1016/j.autcon.2018.05.005.

[5] S. Ghaffar, P. Mullett, Commentary : 3D printing set to transform the construction industry, Struct. Build. (2018) 1–2, https://doi.org/10.1680/jstbu.18.00136.

[6] A. Paolini, S. Kollmannsberger, E. Rank, Additive manufacturing in construction : a review on processes , applications , and digital planning methods, Addit. Manuf. 30 (2019) 100894, https://doi.org/10.1016/j.addma.2019.100894.

[7] B. Khoshnevis, Automated construction by contour crafting - related robotics and information technologies, Autom. ConStruct. 13 (2004) 5–19, https://doi.org/10.1016/j.autcon.2003.08.012.

[8] F. Bos, R. Wolfs, Z. Ahmed, T. Salet, Additive Manufacturing of Concrete in Construction : Potentials and Challenges of 3D Concrete Printing, 2016, p. 2759, https://doi.org/10.1080/17452759.2016.1209867.

[9] R.R.B. Khoshnevis, H. Kwon, S. Bukkapatnam, Crafting large prototypes, IEEE Robot. Autom. Mag. (2001) 33–42, https://doi.org/10.1109/100.956812.

[10] R.A. Buswell, A. Thorpe, R.C. Soar, A.G.F. Gibb, Design, data and process issues for mega-scale rapid manufacturing machines used for construction, Autom. ConStruct. 17 (2008) 923–929, https://doi.org/10.1016/j.autcon.2008.03.001.

[11] N. Labonnote, A. Rønnquist, B. Manum, P. Rüther, Additive construction: state-of-the-art, challenges and opportunities, Autom. ConStruct. 72 (2016) 347–366, https://doi.org/10.1016/j.autcon.2016.08.026.

[12] P. Shakor, S. Nejadi, G. Paul, S. Malek, Review of emerging additive manufacturing technologies in 3D printing of cementitious materials in the construction industry, Front. Built Environ. 4 (2019) 85, https://doi.org/10.3389/fbuil.2018.00085.

[13] P. Shakor, S. Nejadi, G. Paul, A study into the effect of different nozzles shapes and fibre-reinforcement in 3D printed mortar, Materials (Basel) 12 (2019), https://doi.org/10.3390/MA12101708.

[14] B. Zhu, J. Pan, B. Nematollahi, Z. Zhou, Y. Zhang, J. Sanjayan, Development of 3D printable engineered cementitious composites with ultra-high tensile ductility for digital construction, Mater. Des. 181 (2019) 108088, https://doi.org/10.1016/j.matdes.2019.108088.

[15] W.R. Leal da Silva, H. Fryda, J.N. Bousseau, P.A. Andreani, T.J. Andersen, Evaluation of early-age concrete structural build-up for 3D concrete printing by oscillatory rheometry, Adv. Intell. Syst. Comput. 975 (2020) 35–47, https://doi.org/10.1007/978-3-030-20216-3_4.

[16] A. Kazemian, X. Yuan, R. Meier, B. Khoshnevis, Performance-Based Testing of Portland Cement Concrete for Construction-Scale 3D Printing, Elsevier Inc., 2019, https://doi.org/10.1016/b978-0-12-815481-6.00002-6.

[17] M.J. Al-Kheetan, S.H. Ghaffar, O.A. Madyan, M.M. Rahman, Development of low absorption and high-resistant sodium acetate concrete for severe environmental conditions, Construct. Build. Mater. 230 (2020) 117057, https://doi.org/10.1016/j.conbuildmat.2019.117057.

[18] M.J. Al-Kheetan, M.M. Rahman, S.H. Ghaffar, M. Al-Tarawneh, Y.S. Jweihan, Comprehensive investigation of the long-term performance of internally integrated

concrete pavement with sodium acetate, Results Eng 6 (2020) 100110, https://doi.org/10.1016/j.rineng.2020.100110.

[19] Y. Wu, B. Lu, T. Bai, H. Wang, F. Du, Y. Zhang, L. Cai, C. Jiang, W. Wang, Geopolymer, green alkali activated cementitious material: synthesis, applications and challenges, Construct. Build. Mater. 224 (2019) 930–949, https://doi.org/10.1016/j.conbuildmat.2019.07.112.

[20] B.B. Jindal, Investigations on the properties of geopolymer mortar and concrete with mineral admixtures: a review, Construct. Build. Mater. 227 (2019) 116644, https://doi.org/10.1016/j.conbuildmat.2019.08.025.

[21] Y.H.M. Amran, R. Alyousef, H. Alabduljabbar, M. El-Zeadani, Clean production and properties of geopolymer concrete; A review, J. Clean. Prod. 251 (2020) 119679, https://doi.org/10.1016/j.jclepro.2019.119679.

[22] M. Chougan, S. Hamidreza Ghaffar, M. Jahanzat, A. Albar, N. Mujaddedi, R. Swash, The influence of nano-additives in strengthening mechanical performance of 3D printed multi-binder geopolymer composites, Construct. Build. Mater. 250 (2020) 118928, https://doi.org/10.1016/j.conbuildmat.2020.118928.

[23] S. Kashif, U. Rehman, Z. Ibrahim, M. Jameel, S.A. Memon, M.F. Javed, M. Aslam, K. Mehmood, S. Nazar, Assessment of rheological and piezoresistive properties of graphene based cement composites, Int. J. Concr. Struct. Mater. (2018), https://doi.org/10.1186/s40069-018-0293-0.

[24] M. Chougan, E. Marotta, F.R. Lamastra, F. Vivio, G. Montesperelli, U. Ianniruberto, A. Bianco, A systematic study on EN-998-2 premixed mortars modified with graphene-based materials, Construct. Build. Mater. 227 (2019) 116701, https://doi.org/10.1016/j.conbuildmat.2019.116701.

[25] F. Celik, H. Canakci, An investigation of rheological properties of cement-based grout mixed with rice husk ash (RHA), Construct. Build. Mater. 91 (2015) 187–194, https://doi.org/10.1016/j.conbuildmat.2015.05.025.

[26] A. Bhowmick, S. Ghosh, Effect of synthesizing parameters on workability and compressive strength of Fly ash based Geopolymer mortar 3 (2012) 168–177, https://doi.org/10.6088/ijcser.201203013016.

[27] J. Xie, J. Wang, R. Rao, C. Wang, C. Fang, Effects of combined usage of GGBS and fly ash on workability and mechanical properties of alkali activated geopolymer concrete with recycled aggregate, Compos. Part B. 164 (2019) 179–190, https://doi.org/10.1016/j.compositesb.2018.11.067.

[28] A. Lampropoulos, A. Cundy, Effect of alkaline activator, water, superplasticiser and slag contents on the compressive strength and workability of slag-fly ash based geopolymer mortar cured under ambient temperature, International Journal of Civil, Environmental, Structural, Construction and Architectural Engineering 10 (2016) 308–312. http://publications.waset.org/10003905/pdf.

[29] H. Alghamdi, S.A.O. Nair, N. Neithalath, Insights into material design, extrusion rheology, and properties of 3D-printable alkali-activated fly ash-based binders, Mater. Des. 167 (2019) 107634, https://doi.org/10.1016/j.matdes.2019.107634.

[30] B. Panda, S.C. Paul, L.J. Hui, Y.W.D. Tay, M.J. Tan, Additive manufacturing of geopolymer for sustainable built environment, J. Clean. Prod. 167 (2018) 281–288, https://doi.org/10.1016/j.jclepro.2017.08.165.

[31] A. Peled, S.P. Shah, Processing effects in cementitious Composites: extrusion and casting. https://doi.org/10.1061/(ASCE)0899-1561(2003)15:2(192), 2003, 192-199.